



## Some manufactured solutions for verification of fluid-structure interaction codes

S. Étienne \*, A. Garon, D. Pelletier

École Polytechnique de Montréal, Canada

### ARTICLE INFO

#### Article history:

Received 30 June 2010

Accepted 16 April 2012

Available online 17 May 2012

#### Keywords:

Fluid-structure interactions

Method of manufactured solutions

Verification

Finite-element method

### ABSTRACT

This paper presents manufactured solutions (MS) for verification of a fluid-structure interactions code. MS provide benchmark solutions for direct evaluation of the solution errors. The method of manufactured solutions (MMS) is a straight forward and general procedure for generating exact analytical solutions with a sufficiently rich structure to ensure that all terms of the differential equations are exercised in the simulations. When used with systematic grid refinement studies, the MMS provides strong code verification with a theorem-like quality. Manufactured solutions for fluid-structure interaction (FSI) problems with large displacements are presented with sample results from grid convergence studies.

© 2012 Elsevier Ltd. All rights reserved.

### 1. Introduction

In the subject of *Quantification of Uncertainty* in numerical simulations, the three most important items are: *Verification of Codes*, *Verification of Calculations* and *Validation* [1]. For logical and practical reasons these activities are performed in this order. **Verification of a code involves error evaluation from a known solution to establish that the numerical code works correctly. Verification of a calculation involves error estimation to make sure that the code delivers the expected accuracy on a specific application problem.**

The agreement of the mathematical model with the physical system of interest is the concern of *Validation*. *Verification* is concerned with solving the equations *right* (doing good numerical analysis) while *Validation* focuses on solving the *right* equations (doing good engineering). Several *Validation* tests with increasing complexity can be found in Bathe and Ledezma [2] and Bathe and Zhang [3].

Journal policy statements used to refer only to *Validation of Calculations* [4]; the assumption made that the code was correct. This is now changing to reflect common practice and also enhance confidence in computational procedures. **Determining the correctness of a code is best done by systematic grid convergence tests on a problem with a benchmark solution.** The best standard of comparison is an exact analytical solution expressed in terms of simple mathematical function such as **sin**, **exp**, **tanh**, etc. Infinite series are not desirable as they tend to be more trouble to evaluate accurately than the numerical solution itself. **The benchmark solution should not only be exact, it should also exhibit a complex enough structure to ensure that all terms in the governing equations are**

exercised by the test. This verification step can be done by several ways. Known analytical solutions or numerically established solutions (see [5]) to a physically realistic problem and converging to it, or manufactured solutions have been used for a long time. All of these three methods have their merits.

In this paper, we focus on the method of manufactured solutions. The terminology, method of manufactured solutions or MMS was coined by Steinberg and Roache [6]. Manufactured solutions, while not called that way, have been developed earlier in structural stress computational procedures [7] for example. For computational fluid dynamics, the method was detailed for complex flow problems by Pelletier and Roache [8,9]. Eça and Hoekstra present manufactured solutions for several 1 and 2 equations models of turbulence [10]. They also demonstrate the verification procedure for these models [11]. An exhaustive discussion may be found in [12,13]. Salari and Knupp [14] demonstrate how sensitive the MMS can be and how useful it is in debugging codes. They have exercised the MMS in a blind study, in which one author modified a CFD code, developed and verified by the other, deliberately introducing errors. The code author then tested the sabotaged code with the MMS. The code used for this exercise was a full time-dependent, compressible and incompressible, Navier–Stokes solver with plenty of options for the user. In all, 21 cases were studied including one *placebo* (no mistake introduced) and several cases including something other than the solution (wrong time step, post-processing errors etc.). The exercise also highlights some of the limitations of the MMS. All order-of-accuracy mistakes errors (all that could prevent the governing equations from being correctly solved) were successfully detected.

This paper proposes a procedure to develop difficult nonlinear fluid-structure interactions (FSI) manufactured solutions for incompressible viscous flows over deforming structures. These problems

\* Corresponding author.

E-mail address: [stephane.etienne@polymtl.ca](mailto:stephane.etienne@polymtl.ca) (S. Étienne).

require an adequately coupled FSI solver to be solved. The paper is organized as follows: after some remarks on MMS, we describe briefly the numerical solution procedure used here. Finally, we describe a procedure to construct MS for fluid-structure interactions modeled using incompressible Navier–Stokes flow and large displacement elasticity. We then demonstrate its usefulness for fluid-structure code verification. Both steady and unsteady solutions are sought and numerical applications are solved via the finite element method.

## 2. The method of manufactured solutions

The method of manufactured solutions (MMS) provides a general procedure for generating analytical solutions for verification of code accuracy. The procedure is very simple (some will say deceptively so!). We first pick a continuum solution. In general this solution will not satisfy the governing equations because of the arbitrary nature of our choice. An appropriate source term is defined to cancel out any imbalance in the PDE caused by our choice of the continuum solution. Interestingly enough, this choice can often be made independently of the code or of the equations considered. That is, we can pick a solution and use it to verify an incompressible Navier–Stokes code, a Darcy flow model, a heat equation, a materials code, etc.

The solution should be non-trivial in the sense that it exercises all derivatives in the PDE. The solution also defines the boundary conditions in all forms (Dirichlet, Neumann or Robin). Such non-trivial analytic solutions can be used to Verify a Code by performing systematic grid convergence studies. This is based on the behavior of the error  $E$  as the mesh size  $\delta$  is reduced (i.e. the asymptotic behavior):

$$E = f_h - f_{ex} = c\delta^p + \text{H.O.T.}, \quad (1)$$

where  $f_{\Delta x}$  is the discrete solution,  $f_{ex}$  the exact solution,  $c$  a constant,  $\delta$  a measure of the discretization, and  $p$  the convergence rate of the numerical scheme. This behavior applies to every consistent methodology (FDM, FVM, FEM etc.). The idea is to monitor the behavior of  $E$  as the grid is refined. Grid doubling is not necessary, just refinement. However, thorough iterative convergence is required. Theoretically, values of  $C = E/\delta^p$  should become constant as the grid is refined.

The procedure will detect all ordered errors (interior discretization, boundary condition discretization etc.). It will not evaluate the adequacy of non ordered approximation such as the distance to an outflow boundary or  $\partial p/\partial n = 0$  at a wall. The errors of such approximations do not vanish as  $\delta \rightarrow 0$ , hence they are *non-ordered approximation*. However, if the code uses a second order approximation of  $\partial p/\partial n = 0$  at a wall and the MMS procedure shows that it is indeed second order accurate, then the code is verified on this point. Note that the method will not detect coding mistakes that slow down the iterative solver while leaving the solution and grid convergence rate unaffected. See Roache [1] for further discussion.

When this grid convergence test is completed satisfactorily, we have verified: any equation transformation used (body fitted grids), the order of the discretization, the coding of the discretization and the matrix solution procedure. Thus, the MMS is a very powerful technique. Users sometimes say that the method is too sensitive, revealing minor inconsistencies in the special treatment of a single grid point that may corrupt the convergence rate of the method everywhere [1]. The complexity of algebraic manipulation needed to evaluate the expression of the source terms may be something of a challenge. However, symbolic manipulation can easily deal with it (i.e. using MAPLE or MATHEMATICA).

Code verification guarantees that the numerical implementation is correct. However, when applying a verified code to a

practical case, one must again perform grid refinement studies to ensure that the code is used correctly. This is called Verification of calculation. Error estimates may be computed using either a classical Richardson extrapolation [1] or any unstructured mesh error estimator [15]. Results from such grid refinement studies are best reported using error bands or the grid convergence index (GCI) for structured meshes [1] or upper and lower bounds of the GCI for unstructured grids [16].

## 3. Equations involved in the fluid-structure verification process

The flow is described by the Navier–Stokes equations (2) and (3) for an incompressible Newtonian fluid.

$$\text{Continuity : } \nabla \cdot \mathbf{u} = 0 \quad \text{on } \Omega^f, \quad (2)$$

$$\begin{aligned} \text{Momentum : } \rho_f \frac{\partial \mathbf{u}_f}{\partial t} + \rho_f (\mathbf{u}_f \cdot \nabla) \mathbf{u}_f &= \nabla \bar{\sigma}_f + \rho_f \mathbf{f}_f \quad \text{on } \Omega^f \\ \text{with } \bar{\sigma}_f &= \mu_f [\nabla \mathbf{u}_f + (\nabla \mathbf{u}_f)^T] - p_f \bar{\mathbf{I}}, \end{aligned} \quad (3)$$

where  $\mathbf{u}_f$  is the velocity in the fluid,  $\bar{\sigma}_f$  the viscous stress tensor,  $p_f$  the fluid pressure and  $\mathbf{f}_f$  a body force, and in our case a source term that will equilibrate the momentum equations from the unbalance generated by the manufactured solution. Such a source term is defined by the user through user subroutines or functions for most of the codes. These equations are supplemented with the following boundary conditions

$$\bar{\sigma}_f \cdot \mathbf{n}_f = \bar{\mathbf{t}}_f \quad \text{on } \Gamma_N^f \quad (\text{Neumann-type}), \quad (4)$$

$$\mathbf{u}_f = \bar{\mathbf{u}}_f \quad \text{on } \Gamma_D^f \quad (\text{Dirichlet-type}). \quad (5)$$

Eq. (4) represents surface forces applied on the portion  $\Gamma_N^f$  of the boundary equation (5) is the inflow condition.

For the structure we consider an isotropic hyperelastic solid undergoing large displacements described by a St.Venant–Kirchhoff material. For geometric nonlinearity in the total Lagrangian approach, the equilibrium equations are expressed on the initial undeformed configuration (subscript 0).

$$\begin{aligned} \rho_s \frac{\partial^2 \boldsymbol{\chi}_s}{\partial t^2} + \nabla \cdot \bar{\boldsymbol{\sigma}}_l &= \rho_s \mathbf{f}_s \quad \text{on } \Omega_s^0 \\ \text{with } \bar{\boldsymbol{\sigma}}_l &= \bar{\mathbf{F}} \cdot \bar{\boldsymbol{\sigma}}_k, \end{aligned} \quad (6)$$

$$\begin{aligned} \bar{\mathbf{F}} &= \bar{\mathbf{I}} + \nabla \boldsymbol{\chi}_s, \\ \bar{\boldsymbol{\sigma}}_k &= \lambda_s \text{tr}(\mathbf{E}_l) \mathbf{I} + 2\mu_s \mathbf{E}_l \quad (\text{St.Venant-Kirchhoff}), \\ \mathbf{E}_l &= (\nabla \boldsymbol{\chi}_s + \nabla \boldsymbol{\chi}_s^T + \nabla \boldsymbol{\chi}_s^T \cdot \nabla \boldsymbol{\chi}_s)/2, \end{aligned}$$

in which  $\boldsymbol{\chi}_s$  is the displacement vector,  $\bar{\boldsymbol{\sigma}}$  the Lagrangian stress tensor,  $\mathbf{f}_s$  a body force,  $\mathbf{F}$  the deformation gradient tensor,  $\mathbf{E}$  the Green–Lagrange strain tensor,  $\bar{\boldsymbol{\sigma}}_k$  the 2nd Piola–Kirchoff stress tensor. The following boundary conditions are imposed on the undeformed configuration

$$\bar{\boldsymbol{\sigma}}_l \cdot \mathbf{n}_s = \bar{\mathbf{t}}_s \quad \text{on } \Gamma_{0,N}^f \quad (\text{Neumann – type}), \quad (7)$$

$$\boldsymbol{\chi}_s = \bar{\boldsymbol{\chi}}_s \quad \text{on } \Gamma_{0,D}^s \quad (\text{Dirichlet – type}). \quad (8)$$

Finally, the fluid–solid interface must be in equilibrium. We require continuity of the surface forces between the fluid and the solid at the interface location. Details on how we match the Eulerian flow and total Lagrangian structural interface equilibrium may be found in Etienne and Pelletier [17]:

$$\mathbf{u}_f = \mathbf{u}_s \quad \text{on } \Gamma_{FS}, \quad (9)$$

$$\bar{\boldsymbol{\sigma}}_c \cdot \mathbf{n}_s + \bar{\boldsymbol{\sigma}}_f \cdot \mathbf{n}_f = 0 \quad \text{on } \Gamma_{FS}. \quad (10)$$

where  $\bar{\boldsymbol{\sigma}}_c$  and  $\bar{\boldsymbol{\sigma}}_f$  are the Cauchy solid and fluid stress tensors, respectively and (9) is the no-slip Dirichlet condition on the fluid–structure interface.

We have opted to not use source terms in interface equilibrium equations while it constitutes a non-trivial exercise. Using source terms in the interface conditions results in a simpler path to generate MS. Indeed, interface source terms makes it easy to specify the MS independently in the fluid and solid zones. Any imbalance in the interface can be fixed with an appropriate source term. But, there are many reasons not to do so.

- Generally, in most codes there is no option for the user to add a source term to the interface equilibrium equations.
- Source terms at the interface must be compatible with the implementation. For FE methods, this requires evaluating source terms in the form of reaction forces which necessitates substantial modifications to the code.
- Another solution could be to add Neumann boundary conditions on either side of the interface. This too, requires adding source terms in the form of normal forces on the deformed boundary on the fluid side. This may be a tricky operation at best; or often a next to impossible task. The user may simply not be authorized to define both Neumann and interface conditions on the same boundary or the code may simply not support such an approach.

We are thus left with the present approach for the development of a coupled fluid-structure MS.

#### 4. Numerical method synopsis

Steady and unsteady fluid-structure interaction problems are solved by a finite element method. In both cases, a monolithic and implicit methodology is used. Nonlinearities are handled with Newton's method. The fluid velocity and pressure and the structural velocity and displacements are discretized with a suitable finite element scheme. For the flow, we opt for the Taylor-Hood element or P2-P1 triangular element which uses quadratic polynomials for velocity and linear polynomials for pressure. It also satisfies the Brezzi compatibility condition between velocity and pressure approximation in incompressible flows. It is 2nd order accurate for the velocity in  $H^1$  norm and 2nd order accurate for the pressure in  $L_2$  norm. The mixed or Lagrange multiplier formulation is used to solve for the velocity and pressure in a coupled manner. For the structural components, we use P2 triangular elements for both the solid velocity and the displacements. Both discretizations are 2nd order accurate in  $H^1$  norm. Transfer of loads between the fluid and the structure is handled via the implicit reaction method (see e.g. Etienne and Pelletier [18]).

For unsteady FSI, we use an arbitrary-Lagrangian Eulerian formulation. Satisfaction of the so-called geometric conservation law (GCL) is essential for successful simulation. The GCL states, as a minimum, that a uniform flow must be solved exactly on deforming domains. An optimal implementation of the GCL will be such that the fixed mesh temporal accuracy is preserved on the deforming domain. Such verification of the code has already been presented in Etienne et al. [19].

#### 5. Steady-state fluid-structure interactions manufactured solutions

In this section, we present a generic methodology to obtain manufactured solutions for a class of steady laminar FSI problems. This methodology applies equally well to cartesian or axisymmetric coordinate systems. We begin with the description of the procedure for 2D problems. This is followed by a numerical example.

Because the flow is incompressible, we seek an MS with a solenoidal velocity field (i.e. continuity equation on the deformed fluid

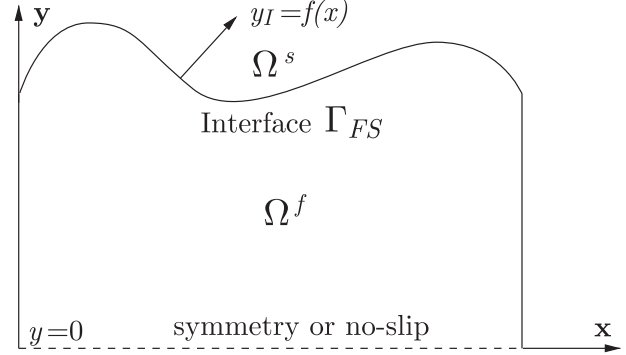


Fig. 1. Arbitrary two-dimensional fluid-structure domain.

domain). Notations and geometry are given on Fig. 1. In general, such a field will not satisfy the momentum equations. Source terms,  $\mathbf{f}_f$  and  $\mathbf{f}_s$  are added to the steady momentum equations (3) and (6), to ensure equilibrium [1]. This is a challenging problem for domains with complex geometry. Furthermore, the flow and structural displacements field must also satisfy boundary conditions on the interface and symmetry axis. Continuity of tractions, equality of displacements and no-slip must be satisfied at the interface. Fortunately, we have some freedom in choosing the boundary condition on the bottom boundary. Imposing no-slip yields a 2D asymmetric channel while no penetration models half a channel.

##### 5.1. A steady 2D fluid-structure interaction manufactured solution procedure

Fig. 1 presents the general setting and notation of our choice of a deformed geometry of a two-dimensional fluid domain. We impose that the chosen solution must be divergence free and such that

$$u = 0 \quad \text{on } y = y_I, \quad (11)$$

$$v = 0 \quad \text{on } y = y_I, \quad (12)$$

$$v = 0 \quad \text{on } y = 0. \quad (13)$$

To begin the construction of our manufactured solution we pick a polynomial expression for the  $y$  component of the velocity which must satisfy conditions (12) and (13). Our choice is

$$v(x, y) = y^k(f(x) - y)G(x) \quad (14)$$

with  $k$  an integer and  $f(x) \in C^3([x_{min}, x_{max}])$  a function describing the geometry of the upper boundary with sufficient smoothness for proper evaluation of source terms. The function  $G(x)$  provides enough flexibility to satisfy the continuity equation and still admit a non trivial  $y$  velocity profile which leads to the following solenoidal velocity field

$$u(x, y) = (k+1)y^k[M[f(x)] - M(y)] - ky^{k-1}[L[f(x)] - L(y)], \quad (15)$$

$$v(x, y) = y^k(f(x) - y)K[f(x)]f'(x), \quad (16)$$

with  $f(x)$  being the supplied deformed interface boundary,  $K(x)$  a user supplied function and  $k$  a user supplied exponent. For  $k \leq 1$ , the resulting profile  $u$  is non zero along the bottom boundary; while, taking  $k > 1$  generates a no-slip condition. We have  $M(x) = \int_0^x K(z)dz$  and  $L(x) = \int_0^x K(z)dz$ . Expressions (15) and (16) for the velocity field satisfy the continuity equation (2), the no-slip condition on the upper wall of arbitrary shape  $f(x)$  and no-slip condition on the lower wall if  $k > 1$ . However, they do not satisfy the momentum equation (3). An appropriate source term  $\mathbf{f}_f$  is introduced to ensure equilibrium as described in Section 3.

We now show two MS flow fields with various shapes of the upper boundary shape  $f(x)$ , the coefficient  $k$  and the function  $K(x)$ . The manufactured velocity field is taken as defined by Eqs. (15) and (16) with *ad hoc* manufactured pressure and viscosity field:

$$\begin{aligned} \mathbf{u}_M &= \{u, v\} \quad \text{and} \quad p_M(x, y) = x^2 + y^2 \quad \text{and} \\ \mu_M &= (1 + x^2 + y^2)/10. \end{aligned} \quad (17)$$

The source term in Eq. (3) is determined to cancel out any imbalance in the PDE caused by our choice of the manufactured solution.

$$\begin{aligned} \rho_f \mathbf{f}_f &= \rho_f \frac{\partial \mathbf{u}_M}{\partial t} + \rho_f (\mathbf{u}_M \cdot \nabla) \mathbf{u}_M + \nabla p_M \\ &\quad - \nabla \cdot [\mu_M (\nabla \mathbf{u}_M + \nabla \mathbf{u}_M^\top)]. \end{aligned} \quad (18)$$

The Navier–Stokes equations with the above source terms are solved by an adaptive finite element method. The adaptive remeshing procedure is very efficient and cost-effective approach for performing grid refinement studies. It relieves the user from the tedious task of generating suitable grids. The error in the velocity field is measured in the energy norm defined as follows

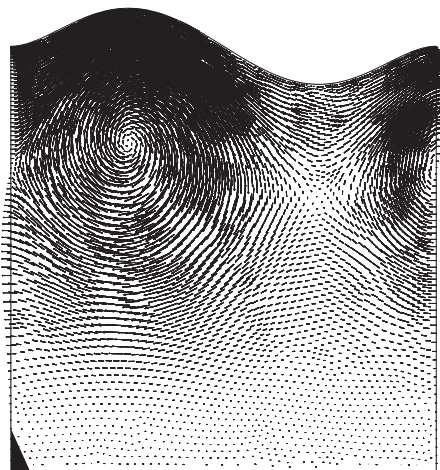
$$\|e_u\|_E^2 = \|\mathbf{u}_{ex} - \mathbf{u}_h\|_E^2 = \int_{\Omega} (\boldsymbol{\tau}_{f,ex} - \boldsymbol{\tau}_{f,h}) : (\boldsymbol{\tau}_{f,ex} - \boldsymbol{\tau}_{f,h}) d\Omega, \quad (19)$$

where  $\boldsymbol{\tau}$  is the usual viscous stress tensor in the fluid. In solid regions we use a similar expression using the linear component of the solid stresses omitting the contributions due to the geometric nonlinearities. The energy norm is equivalent to the usual  $H^1$  semi-norm of the fluid velocity or solid displacements. The pressure error is measured in  $L_2$  norm as follows

$$\|e_p\|_{L_2}^2 = \|p_{ex} - p_h\|_{L_2}^2 = \int_{\Omega} (p_{ex} - p_h)^2 d\Omega. \quad (20)$$

In the above expression subscripts *ex* refers to the exact solution (manufactured) and *h* identifies the finite element solution.

The same norms are used for the error estimators, the only difference is that the exact solution is replaced by a local reconstruction (projection) of the solution (i.e. a Zhu–Zienkiewicz error estimator [15]).



(a) Velocity vector field

**Example 1.** For our first example we set

$$\begin{aligned} k &= 4 \quad \text{and} \quad K(x) = x^4 \quad \text{and} \quad f(x) \\ &= 1 + 10x^2(x - 1/2)(x - 1)^2. \end{aligned} \quad (21)$$

Fig. 2(a) shows the geometry of the domain induced by the above choice for  $k$ ,  $K(x)$  and  $f(x)$ . The figure also shows the velocity field  $\mathbf{u}_M$  of the manufactured solution after the fourth adaptive cycle. Fig. 2(b) presents grid convergence results of the velocity and pressure fields with adaptive refinement. On each graph there are 2 curves, the solid one is the norm of the true errors  $\|\mathbf{u}_{ex} - \mathbf{u}_h\|$ ,  $\|p_{ex} - p_h\|$  while the dashed ones are the error estimators  $\|\mathbf{u}^* - \mathbf{u}_h\|$  and  $\|p^* - p_h\|$  where the asterisk identifies that a reconstructed field is used in lieu of the exact field.

As can be seen the true errors of velocity and pressure decrease with adaptive grid refinement. Also, the error estimators appear to converge to the true error. Thus, the efficiency index  $\theta = \|\mathbf{u}^* - \mathbf{u}_h\|/\|\mathbf{u}_{ex} - \mathbf{u}_h\|$  tends to a unit value. Similar observations holds for the pressure field indicating that the accuracy of the finite element solution ( $\mathbf{u}_h, p_h$ ) improves with each cycle of mesh adaption. Moreover, they also indicate that the error estimator becomes sharper with adaptive refinement. All four curves exhibit the slope (convergence rate) predicted by theory (more accurate) and hence more reliable with grid adaption.

**Example 2.** For this case we set

$$\begin{aligned} k &= 2, \quad K(x) = x^2, \\ f(x) &= 1 + 400x^2(x - 0.4)(x - 0.6)(x - 0.7)(x - 1)^2. \end{aligned} \quad (22)$$

Fig. 3(a) shows clearly that the geometry of the domain presents more pronounced variations than that of Example 1. Note also that the velocity field presents more evident and pronounced vortices. It also reveals the significant and highly localized grid refinement that takes place between adaptive cycles 4 and 8.

Finally Fig. 3(d) shows the very good convergence of the velocity error and the excellent behavior of its error estimator. The pressure also converges very well to its exact solution:  $\|p_{ex} - p_h\|$  decreases at its theoretical rate. The error estimator also

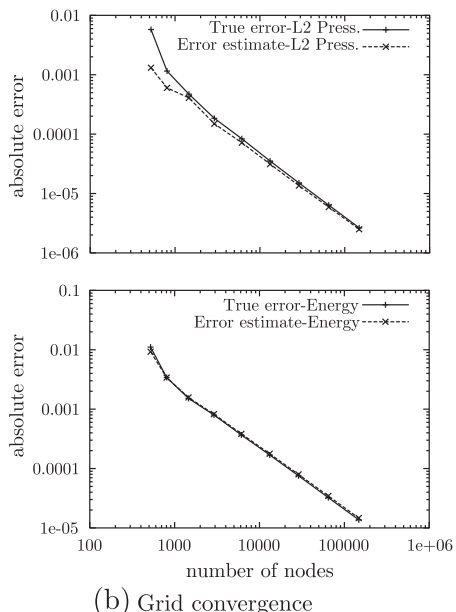
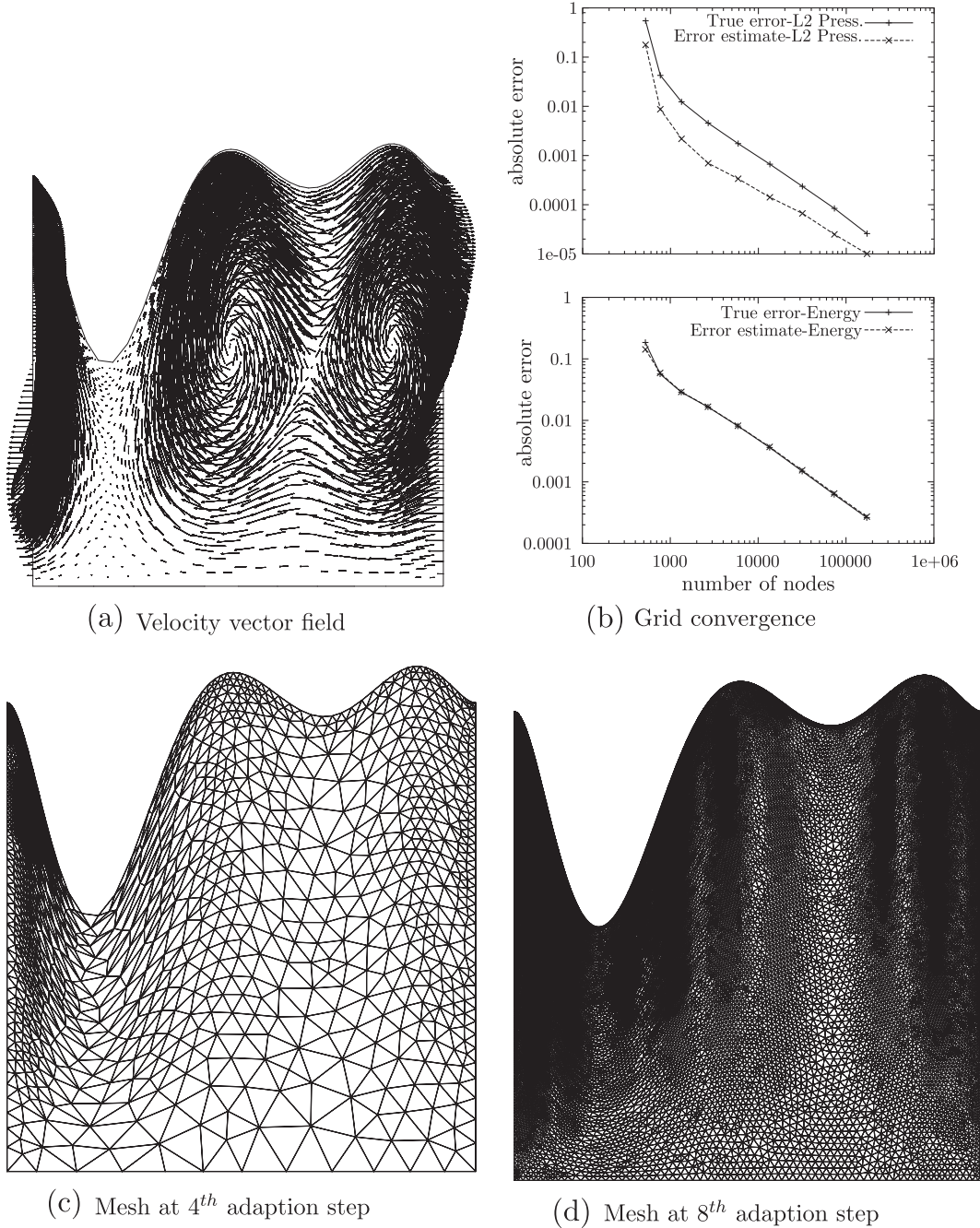


Fig. 2. Flow field and grid convergence for a two-dimensional steady-state flow manufactured solution.



**Fig. 3.** Flow field, grid convergence and selected meshes for a two-dimensional steady flow manufactured solution.

behaves in the same manner. However the distance between the curves for the true pressure error and its estimator appears to remain constant. An indication that the efficiency index asymptotes to a value different from unity.

We now turn our attention on the development of a manufactured displacement field compatible with this fluid domain. The boundary conditions at the fluid–solid interface state that the displacements of the fluid points on the interface must be equal to those of the solid domain. However, the manufactured solution in the solid domain satisfying interface displacements will generally not satisfy the equilibrium equation (6) unless we add a source term obtained from the manufactured displacement field  $\chi_M = [\chi_M, \eta_M]^T$  and equilibrium equation (6),

$$\mathbf{f}_s = \rho_s \frac{\partial^2 \chi_M}{\partial t^2} + \nabla \cdot \bar{\sigma}_l M. \quad (23)$$

Note that since there is no solid equivalent of the fluid continuity equation for  $\mathbf{f}_s$  the development of the MS for the structural component is simpler than that for the fluid. Had the solid material been incompressible (rubber), a procedure analogous to that developed for the flow would have been necessary.

For our purpose we pick the following manufactured displacement field.

$$\xi_M = a(x, y) \quad \text{and} \quad \eta_M = b(x, y)(f(x) - 1). \quad (24)$$

in which  $a(x, y)$ ,  $b(x, y)$  are  $C^3(\Omega_0^s)$  functions. Obviously  $b(x, 1)$  must be equal to 1 to ensure that the structural field will match the fluid–structure interface location and  $a(x, 1)$  may be taken equal to zero at the interface without loss of generality. Functions  $a(x, y)$  and  $b(x, y)$  must however be sufficiently rich to exercise all derivatives in the structural equations.

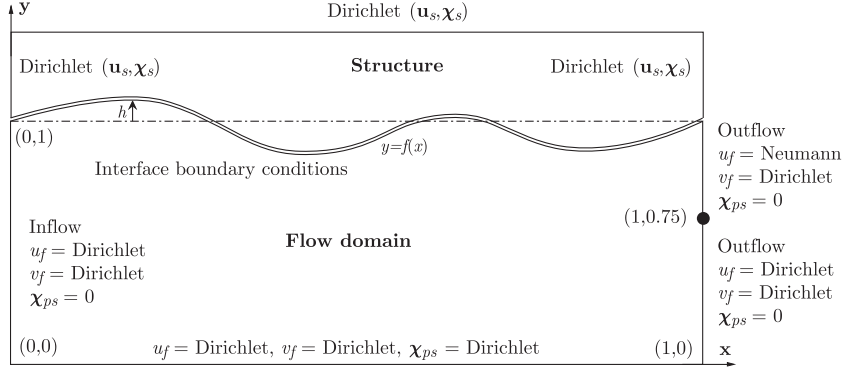


**Fig. 4.** Boundary conditions and geometry for the manufactured solution.

The last step is to ensure continuity of the fluid and solid forces at the fluid–solid interface. This is done by specifying appropriate functions for the pressure and viscosity distributions. Since  $\mathbf{n}_1^f = -\mathbf{n}_1^s$ , we will drop subscripts for the unit normal vectors in Eq. (10) to obtain

$$\bar{\sigma}_c \cdot \mathbf{n} = \bar{\sigma}_f \cdot \mathbf{n}. \quad (25)$$

Expressing Eq. (25) in terms of its  $x$  and  $y$  components yields

$$\sigma_{cx} n_x + \sigma_{cy} n_y = \sigma_{fx} n_x + \sigma_{fy} n_y, \quad (26)$$

$$\sigma_{cy} n_x + \sigma_{cx} n_y = \sigma_{fx} n_x + \sigma_{fy} n_y. \quad (27)$$

Now, let  $S_x = \sigma_{cx} n_x + \sigma_{cy} n_y$  and  $S_y = \sigma_{cy} n_x + \sigma_{cx} n_y$  denote the cartesian components of the forces at the interface, Eqs. (26) and (27) may be written in the following explicit form along

$$S_x = \left( 2\mu_f \frac{\partial u_f}{\partial x} - p_f \right) n_x + \mu_f \left( \frac{\partial u_f}{\partial y} + \frac{\partial v_f}{\partial x} \right) n_y, \quad (28)$$

$$S_y = \mu_f \left( \frac{\partial u_f}{\partial y} + \frac{\partial v_f}{\partial x} \right) n_x + \left( 2\mu_f \frac{\partial v_f}{\partial y} - p_f \right) n_y. \quad (29)$$

The coefficients  $n_x$  and  $n_y$  are the components of the normal to the interface. It is possible to solve these equations to find the expression of pressure and viscosity fields needed to ensure that Cauchy manufactured fluid stresses at the interface location are satisfied. Solving for the pressure and viscosity fields leads to the following expressions along the interface,

$$\mu_f = \frac{S_x n_y - S_y n_x}{-\mathbf{B}n_x^2 - \mathbf{C}n_x n_y + \mathbf{A}n_x n_y + \mathbf{B}n_y^2}, \quad (30)$$

$$p_f = \frac{-\mathbf{A}S_y n_x - \mathbf{B}S_y n_y + \mathbf{B}S_x n_x + \mathbf{C}S_x n_y}{-\mathbf{B}n_x^2 - \mathbf{C}n_x n_y + \mathbf{A}n_x n_y + \mathbf{B}n_y^2}. \quad (31)$$

where  $\mathbf{A} = 2\partial u/\partial x$ ,  $\mathbf{B} = (\partial u/\partial y + \partial v/\partial x)$  and  $\mathbf{C} = 2\partial v/\partial y$  at the interface location.

Thus, the manufactured pressure and viscosity distributions are easily expressed in terms of the fluid velocity, solid displacement and the interface unit normal vector to the deformed interface. Note that the fluid pressure and viscosity depend on  $x$  only. Hence, this MS is not quite as general as one would like because some derivatives are not exercised by that choice, i.e.  $\partial p/\partial y = \partial \mu/\partial y = 0$ . However, the manufactured solutions for the flow do exercise these derivatives. The two manufactured fields for  $\mathbf{u}$  and  $\chi$  are now put together to define the fluid–structure MS.

We now summarize the general expression of the manufactured FSI solutions for 2D steady configurations before proceeding with specific examples.

Given sufficiently smooth functions  $f(x)$ ,  $K(x)$ ,  $a(x,y)$ ,  $b(x,y)$ ,  $k$  an integer,  $E$  and  $\nu$  the Young modulus and Poisson coefficient, a general manufactured solution to the fluid–structure interaction

equations (2,3,6,9,10) is given by the incompressible flow and structural displacement:

$$u(x, y) = (k+1)y^k \{M[f(x)] - M(y)\} - ky^{k-1}\{L[f(x)] - L(y)\},$$

$$v(x, y) = y^k(f(x) - y)K[f(x)]f'(x),$$

$$\mu_f(x) = (S_x n_y - S_y n_x)/(-\mathbf{B}n_x^2 - \mathbf{C}n_x n_y + \mathbf{A}n_x n_y + \mathbf{B}n_y^2),$$

$$p_f(x) = \frac{-\mathbf{A}S_y n_x - \mathbf{B}S_y n_y + \mathbf{B}S_x n_x + \mathbf{C}S_x n_y}{-\mathbf{B}n_x^2 - \mathbf{C}n_x n_y + \mathbf{A}n_x n_y + \mathbf{B}n_y^2},$$

$$M(x) = \int_0^x K(z)dz,$$

$$L(x) = \int_0^x K(z)zdz,$$

$$\xi(x, y) = a(x, 1) \quad \text{with } a(x, 1) = 0,$$

$$\eta(x, y) = b(x, y)(f(x) - 1) \quad \text{with } b(x, 1) = 1,$$

$$\mathbf{A} = 2\partial u/\partial x|_{y=f(x)}, \mathbf{B} = (\partial u/\partial y + \partial v/\partial x)|_{y=f(x)}, \mathbf{C} = 2\partial v/\partial y|_{y=f(x)}.$$

Note that  $S_x$  and  $S_y$  are the Cauchy traction components on fluid–solid interface. They are obtained from the known solid stress solution. However, one can construct more complex fluid pressure and viscosity fields functions of  $x$  and  $y$ .

We now present two applications of this general manufactured solution (MS) for verifying our 2D cartesian implementation of the FSI formulation in our finite element solver. The boundary conditions on the undeformed geometry are depicted on Fig. 4. In the first example (FSI-MS 1) the shape of the interface is given by a non polynomial function. The second one (FSI-MS 2) uses a 7th degree polynomial defining the shape of the interface. Finally, the second example entails a more complex MS for the structural displacements to ensure that all derivatives are exercised.

**Example FSI-MS 1.** For this case, the shape of the interface in the deformed configuration and all user supplied functions and constants are given by

$$f(x) = 1+h[1-\cos(2\pi x)]\sin(2\pi x), \quad h=0.1, \quad k=1, \quad K(x) = x, \quad (32)$$

$$a(x, y) = [1+10h\cos(2\pi x)/3](1-y) \quad \text{and } b(x, y) = 1. \quad (33)$$

We set  $E = 2$  for the Young modulus and the Poisson ratio  $\nu = 0.1$ . As can be observed from Fig. 5(b), there is a negative  $u$  component velocity gradient in the vertical direction at the interface. Positive fluid viscosity induces a positive horizontal friction. To compensate, a negative  $\xi$  gradient in the  $y$  direction is required. This displacement field induces a positive fluid viscosity all along the interface, see Fig. 6(b) and preserves solid integrity, i.e. avoids folding of the solid on itself.

Fig. 5(a) shows the mesh in both media and Fig. 5(b) the velocity field in the fluid domain. Note the strong recirculating nature of the manufactured velocity field.

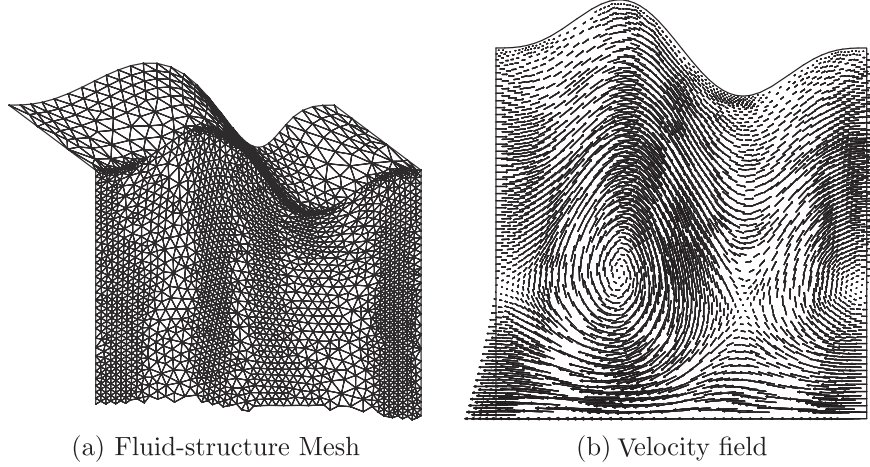


**Fig. 5.** Close-up view of the mesh at interface location and manufactured flow at intermediate mesh refinement.

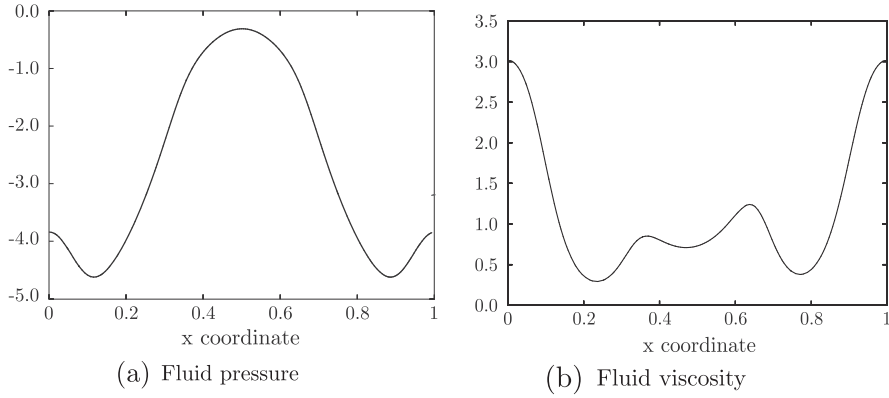


**Fig. 6.** Pressure and viscosity distributions at the interface.

In our choice of FSI-MS, compatible pressure and viscosity distributions are functions of  $x$  only,  $p^m = p(x)$ ,  $\mu^m = \mu(x)$ . The pressure and viscosity profiles are shown on Fig. 6(a) and (b).

Now that the fluid-structure manufactured solution has been presented, we turn our attention to the grid refinement study and the convergence rates of the error. The elemental error contributions from the fluid and solid regions are weighed so as to ensure that the adaptive method will adjust the mesh size in both the fluid and solid regions. Very similar expressions are used to obtain the error in the fluid and in the solid. In fact, we use Eq. (19) for the energy norm of the flow velocity and the following expression for the energy norm of the error in the solid

$$\|e_\chi\|_E^2 = \|\chi_{ex} - \chi_h\|_E^2 = \int_{\Omega} (\tau_{s,ex} - \tau_{s,h}) : (\tau_{s,ex} - \tau_{s,h}) d\Omega. \quad (34)$$

At this point we must note that  $\mathbf{u}$  and  $\chi$  have different units and the material properties in the two sub-domains may differ by several orders of magnitude. Hence their contribution to the error could exhibit differences of several orders of magnitude. For the time being, and for simplicity, we use a linear combination of the velocity and displacement errors to drive the adaptive remeshing process. The weighting coefficients are chosen so that the weight contributions from each subdomain are of the same order of magnitude. This ensures that the adaptive process does not favor the fluid over the solid and vice versa.

The grid convergence for the fully coupled FSI problem is depicted on Fig. 7(a) and (b) for the steady problem. The norm of the velocity/displacement error fields and the L2 norm of the pres-

sure errors both exhibit the theoretically expected quadratic convergence. In agreement with the theoretical a priori estimates of the convergence rate. The Taylor-Hood element is used for the flow and quadratic triangular elements used for structural displacements, all of which are second order accurate in space. The asymptotic convergence rate of the error estimator is equal to those predicted by theory. Thus we conclude that the implementation of the FSI model is correct and thus has been verified.

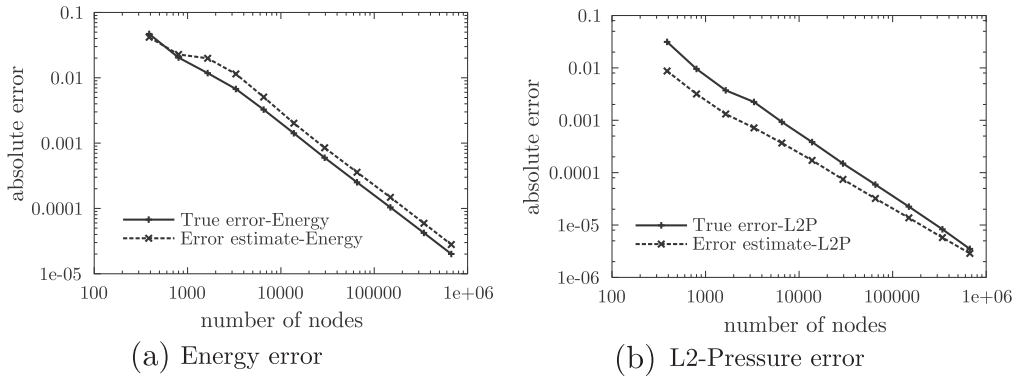
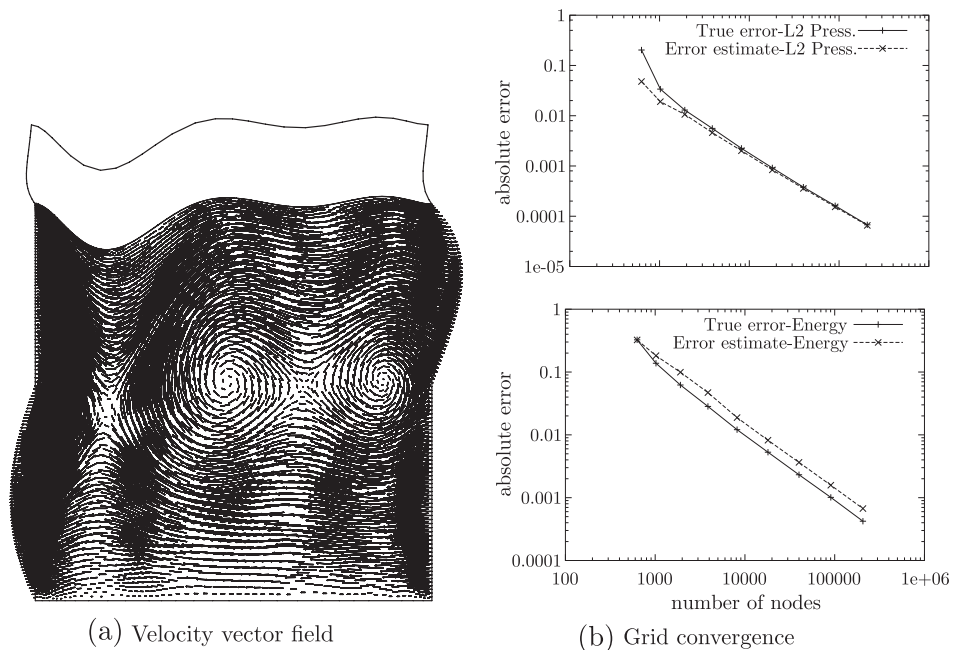
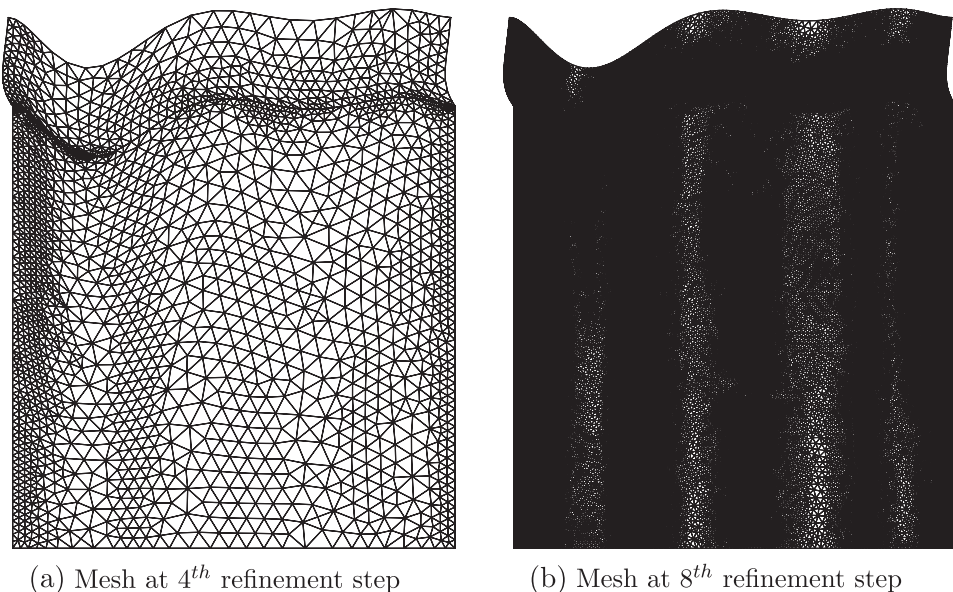
**Example FSI-MS 2.** For this second steady FSI MS, we took the second example of the 2D steady flow MS solution with a modification on the amplitude of the interface displacement. This MS exhibits a more complex velocity field as well as a stiffer structural displacement field. Also, this solution exhibits no-slip at the bottom boundary by having chosen  $k = 2$ . In this case we have

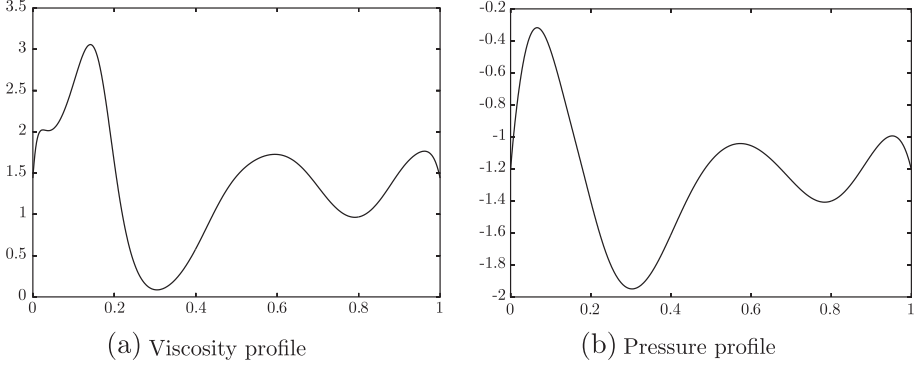
$$f(x) = 1 + 400x^2(x - 0.4)(x - 0.6)(x - 0.7)(x - 1)^2, \quad (35)$$

$$k = 2, \quad K(x) = x^2, \quad (36)$$

$$a(x,y) = -3 \tanh(10(y - 1)) e^{10(1-y)} / 40 \quad \text{and} \quad b(x,y) = 1. \quad (37)$$

Fig. 8(a) shows the velocity vector field at the 4th mesh adaption step. The flow solution presents the particularity of having two vortical structures and two saddle points. Fig. 8(b) shows that the grid refinement results are in agreement with the theoretical expected rates of convergence of  $u$ ,  $p$  and  $\chi$ . Note that this solution is such that all derivatives in the structural domain are exercised due to the sufficient complexity of the structural displacements. Fig. 9(a) and (b) show grids at the 4th and 8th adaption steps. Here again

**Fig. 7.** Grid convergence for two-dimensional steady FSI manufactured solution.**Fig. 8.** Flow field and grid convergence for a 2D steady FSI-MS.**Fig. 9.** Selected meshes for a 2D steady FSI-MS.

Fig. 10. Pressure and viscosity  $x$  profiles for a 2D steady FSI-MS.

vertical bands of refinement appear correlated to the regions of high curvature of the distributions of  $p$  and  $\mu$ . Finally, Fig. 10(a) show viscosity and pressure  $x$  profiles.

### 5.2. A steady axisymmetric fluid-structure manufactured solution procedure

We now present a MS for an axisymmetric frame of reference. We proceed in the same manner as for the two-dimensional cartesian MS. First, we seek a velocity field satisfying the continuity equation and inject it in the momentum equations to determine the body forces  $\mathbf{f}_f$  and  $\mathbf{f}_s$  needed to ensure equilibrium.

Given sufficiently smooth functions  $f(x)$ ,  $K(x)$ ,  $\alpha(z,r)$  and  $\beta(z,r)$ ,  $k$  an integer,  $E$  and  $v$  the Young modulus and Poisson ratio. A general manufactured solution to the fluid-structure interaction equations 2,3,6,9,10 for axisymmetric problems is given by the following incompressible flow and structural displacement fields

$$\begin{aligned} u(z,r) &= (k+2)r^k\{M[f(z)] - M(r)\} - (k+1)r^{k-1}\{L[f(z)] - L(r)\}, \\ v(z,r) &= z^k(f(z) - r)K[f(z)]f'(r), \\ \mu_f(z) &= (S_z n_r - S_r n_z)/(-Bn_z^2 - Cn_z n_r + An_z n_r + Bn_r^2), \\ p_f(z) &= \frac{-AS_r n_z - BS_r n_r + BS_z n_z + CS_z n_r}{-Bn_z^2 - Cn_z n_r + An_z n_r + Bn_r^2}, \\ M(x) &= \int_0^x K(z)dz, \\ L(x) &= \int_0^z K(z)dz, \\ \xi(z,r) &= \alpha(z,r) \quad \text{with } \alpha(z,1) = 0, \\ \eta(z,r) &= \beta(z,r)(f(z) - 1) \quad \text{with } \beta(z,1) = 1, \\ \mathbf{A} &= 2\partial u/\partial z|_{r=f(z)}, \quad \mathbf{B} = (\partial u/\partial r + \partial v/\partial z)|_{r=f(z)}, \quad \mathbf{C} = 2\partial v/\partial r|_{r=f(z)}. \end{aligned}$$

Note that  $S_z$  and  $S_r$  are the Cauchy traction components on the fluid-solid interface. They are obtained from the known solid stress solution with  $n_z$  and  $n_r$ , the components of the normal to the interface.

We apply this MS to the verification of our FE code for steady state axisymmetric fluid-structure interactions. The boundary conditions and the geometry are depicted on Fig. 4 replacing  $y$ 's with  $r$ 's.

We begin by specifying the user supplied functions  $f(z)$ ,  $K(z)$  and the exponent  $k$  to complete the specification of the steady axisymmetric manufactured solution. The shape of the interface in the deformed configuration is

$$k = 1 \quad \text{and} \quad K(z) = 1 \quad \text{and} \quad f(z) = 1 + h\{1 - \cos(2\pi z)\}, \quad (38)$$

$$a(z,r) = \frac{1}{4}(1-r) \quad \text{and} \quad b(z,r) = 1. \quad (39)$$

which leads to the following fluid flow velocity and structural displacement fields:

$$u(z,r) = 3r\{1+h(1-\cos(2\pi z))\} - \{1+h(1-\cos(2\pi z))\}^2 - 2r^2, \quad (40)$$

$$v(z,r) = 2\pi r\{1+h(1-\cos(2\pi z)) - r\} \sin(2\pi z), \quad (41)$$

$$\xi = \frac{1}{4}(1-r) \quad \text{and} \quad \eta = (2-r)h(1-\cos(2\pi z)). \quad (42)$$

Fig. 11(a) shows the mesh at the 4th refinement step and Fig. 11(b) illustrates non-trivial vortical structures for  $h = 0.03$ .

We picked values of 2 and 0.1 for the Young modulus and the Poisson ratio, respectively. The chosen structural displacement field yields the pressure and viscosity distributions shown on Fig. 12.

We now use this solution to verify our adaptive FSI solver. Fig. 13(a) and (b) present results from a grid convergence study performed with our adaptive finite element program. As can be seen, the true and estimated errors decrease with a slope of 2. This confirms second order accuracy in space. Moreover, the estimated error converges to the true error as the mesh is refined. This indicates that the accuracy of the solution and the quantitative reliability of the estimator both improve with adaptive remeshing and verify both the error estimates and the adaptive remeshing algorithm in the sense of Roache et al. [4] (i.e. performs according to theory).

### 6. A 2D unsteady fluid-structure interactions manufactured solution procedure

The difference between steady and unsteady FSI lies in the fact that for an unsteady case the interface velocity is non-zero and varies with time as are velocities, pressure, viscosity in the flow domain and velocities, displacements in the solid domains.

Given sufficiently smooth functions  $f(x,t)$ ,  $K(x,t)$ ,  $a(x,y,t)$ ,  $b(x,y,t)$ ,  $k$  an integer,  $E$  and  $v$  the Young modulus and Poisson coefficient, a general manufactured solution to the fluid-structure interaction equations 2,3,6,9,10 is given by the following incompressible flow and structural displacement fields

$$\begin{aligned} u(x,y,t) &= (k+1)y^k\{M[f(x,t)] - M(y)\} - ky^{k-1}\{L[f(x,t)] - L(y)\}, \\ v(x,y,t) &= y^k(f(x,t) - y)K[f(x,t)]f'(x,t) + \frac{\partial f}{\partial t}(x,t), \\ \mu_f(x,t) &= (S_x n_y - S_y n_x)/(-Bn_x^2 - Cn_x n_y + An_x n_y + Bn_y^2), \\ p_f(x,t) &= \frac{-AS_y n_x - BS_y n_y + BS_x n_x + CS_x n_y}{-Bn_x^2 - Cn_x n_y + An_x n_y + Bn_y^2}, \\ M(x,t) &= \int_0^x K(z,t)dz, \\ L(x,t) &= \int_0^z K(z,t)dz, \\ \xi(x,y,t) &= a(x,y,t) \quad \text{with } a(x,1,t) = 0, \\ \eta(x,y) &= b(x,y,t)(f(x,t) - 1) \quad \text{with } b(x,1,t) = 1, \\ \mathbf{A} &= 2\partial u/\partial x|_{y=f(x,t)}, \quad \mathbf{B} = (\partial u/\partial y + \partial v/\partial x)|_{y=f(x,t)}, \\ \mathbf{C} &= 2\partial v/\partial y|_{y=f(x,t)}. \end{aligned}$$

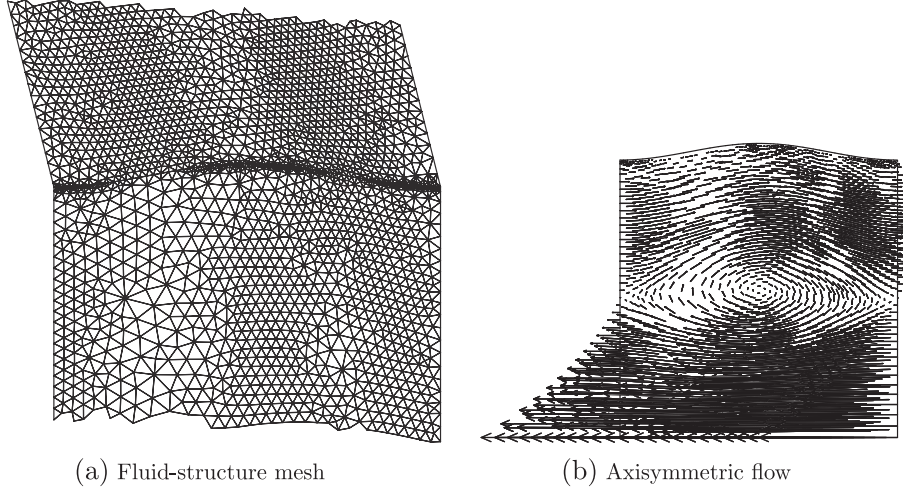


**Fig. 11.** Close-up view of the mesh near the interface and manufactured flow.

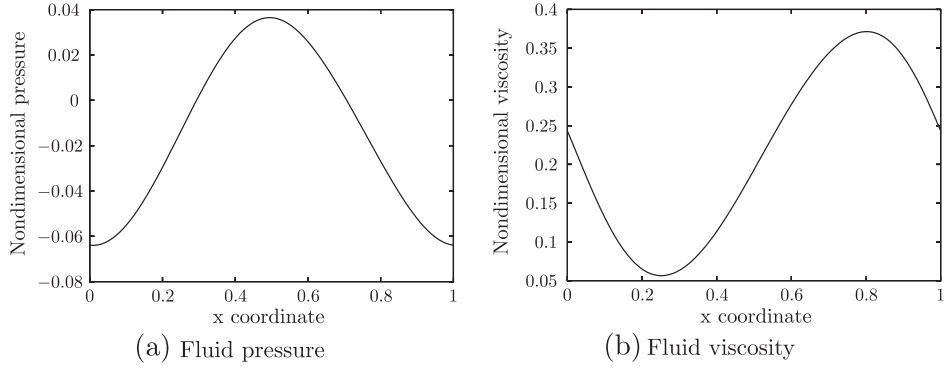


**Fig. 12.** Pressure and viscosity distributions at the interface.

Note that  $S_x$  and  $S_y$  are the Cauchy traction components at the fluid-solid interface. They are obtained from the known solid stress solution with  $n_x$  and  $n_y$  the components of the normal to the interface.

To test this unsteady FSI manufactured solution we have chosen the following expressions for  $f$ ,  $k$ ,  $K$ ,  $a$  and  $b$

$$k = 1 \quad \text{and} \quad K(x, t) = f(x, t) + \{8 - 7(h(t)/h_0)^2\}, \quad (43)$$

$$f(x, t) = 1 + h(t)[1 - c(x)]s(x), \quad (44)$$

$$a(x, y, t) = [1 + 10h(t)c(x)/3](1 - y) \quad \text{and} \quad b(x, y, t) = 1, \quad (45)$$

$$h(t) = h_0 \sin[2\pi(t + t_0)], \quad c(x) = \cos(2\pi x), \quad s(x) = \sin(2\pi x). \quad (46)$$

with  $h(0) = 0.1$ .

We make the following observations. The choice for  $h(t)$  results in a time periodic manufactured solution. By design, the fluid velocity is divergence free. Fluid and solid stresses match at the interface by judiciously choosing the fluid pressure and viscosity values as a function of the normal solid stress at the interface location.

Note that the initial condition corresponds to the first 2D steady MS discussed in Section 5.1. We restart from the steady case with 87,900 nodes. For this unsteady solution we have chosen the first order Euler implicit scheme for both the flow and the structure. Better time integrators are available and have proven to be very effective (see Etienne et al. [19]). However, since the focus of this work is on code verification, it is acceptable to demonstrate the process using the simplest of time integrators without loss of generality.

The solution is advanced in time on the time interval  $[0.25, 0.35]$  starting with one time step  $\Delta t$  that we repeatedly divide by 2, and thus having  $\Delta t_i = 0.1/2^{i-1}$ ,  $i \in [1, 9]$ . The time convergence for the fully coupled FSI problem is depicted on Fig. 14 for the unsteady problem. Errors are evaluated using Eqs. (19) and (20). We observe a clear asymptotic slope of 1 for both velocity and pressure errors as one refines the time step which is the theoretical convergence rate for the Euler implicit scheme. The error in measure is computed the solution at  $t_f$ .

In fact, by using the MS we have verified the flow and structural solver codes implementation, Dirichlet and Neumann BC, spatial and temporal dependence of pressure and viscosity. We have also verified the fluid-structure implicit coupling of the code.

## 7. Conclusion

This paper has presented a detailed description of manufactured solutions for FSI code verification. The MMS produces a rich variety of exact analytical solutions for use as benchmarks in systematic grid refinement tests. Such MS have proven to be remarkably sensitive for code verification. The method is straightforward to implement and use and, when applied to all options combinations in a code, can lead to complete code verification.

In this article, the Galerkin finite element method was used in conjunction with the Taylor-Hood element, the mixed method as well as full ALE-GCL compliance for the flow on time deforming domains. Standard quadratic elements are used for the structure. The MMS was detailed for two-dimensional cartesian and axisym-

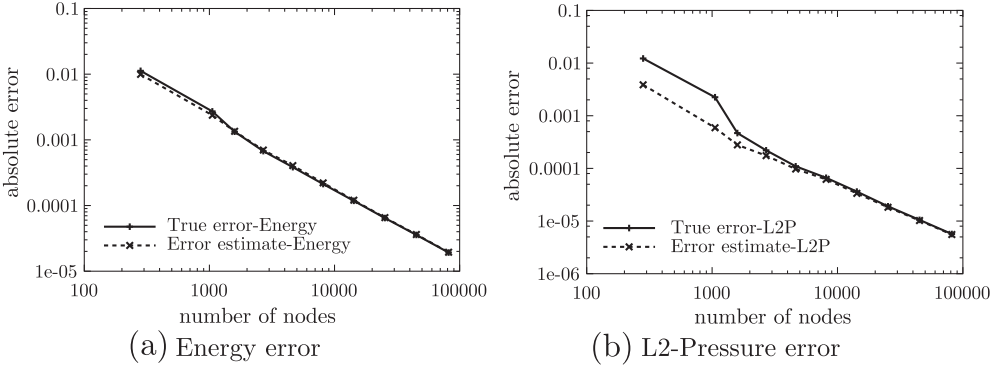


**Fig. 13.** Grid convergence for axisymmetric steady FSI manufactured solution.

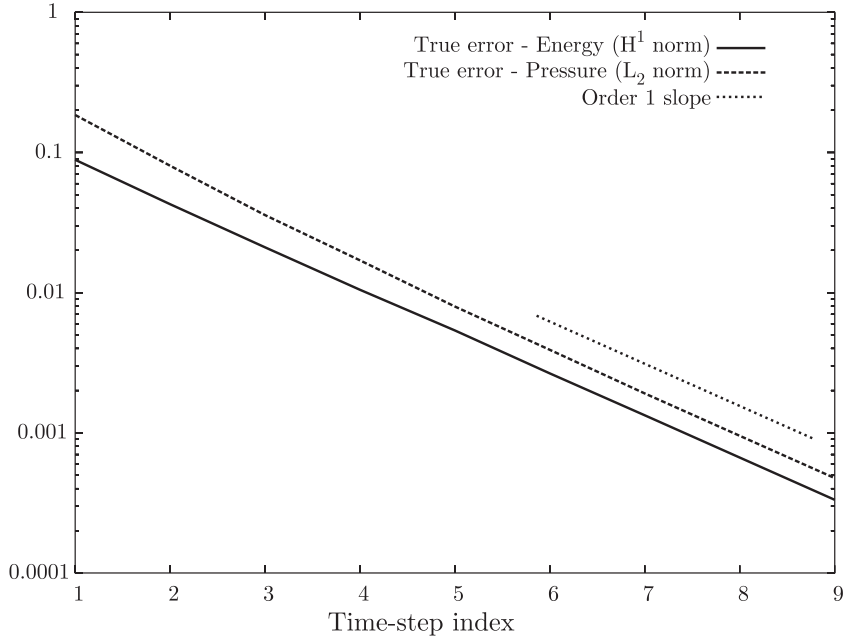


**Fig. 14.** Time-step refinement study, energy and pressure errors as a function of time-step refinement.

metric coordinate systems. Steady and unsteady 2D solutions have been presented whereas only steady axisymmetric solutions have been shown.

Manufactured solutions were presented for incompressible flows interacting with a hyperelastic structure undergoing large displacements. Grid refinement studies using the proposed manufactured solutions reveal that the observed convergence rate is equal to its theoretical value. Thus, the fluid-structure code, the error estimator and the adaptive module are verified in the sense of Roache et al. [4]. A Zhu-Zienkiewicz error estimator was employed to compute error estimates. These errors were compared to the exact error. We have been able to validate the second order space precision of the whole fluid-structure model and the implementation of the error estimator for steady computations.

Unsteady computations are more challenging as both time and space discretization contribute to the error. We assumed that the temporal accuracy is the controlling aspect. Indeed, in our example, we selected a sufficiently fine mesh to ensure that spatial error remains far below temporal error and do not pollute the apparent convergence rate of the time scheme.

The quadratic convergence of Newton's method has been observed when the fully coupled strategy is used. That is part of the verification process. Indeed a linear convergence history would

support that this portion of the algorithm is not fully coupled. Note that to mimick the decoupled strategy we have decoupled the fluid flow and the mesh deformation. The decoupled strategy was as follows, for each Newton iteration, we solved for the structure then for the flow and started another Newton iteration until convergence is reached or the algorithm breaks down. For each Newton iteration, interface boundary conditions came from the preceding iteration. For steady solutions, this decoupling prevented us from getting a solution. The Newton procedure diverged while starting from a close approximation of the solution. This demonstrates the stiff nature of these manufactured FSI solutions. However, this decoupled strategy is not state-of-the art and more advanced and robust coupling algorithms for partitioned fluid-structure interaction simulations exist, e.g. Interface GMRES [20], Aitken relaxation [21] and Interface quasi-Newton [22].

The MS for FSI presented herein have been designed in such a way that no source terms is added to the continuity equation for the fluid and to the interface equations. This means that body forces are needed only for the flow momentum and solid equations. It is thus applicable to any other FSI code.

How it helps code development and maintenance? It contributes to test the robustness of the code since the degree of complexity of a solution can be parameterized. It simplifies code

maintenance by limiting the number of test cases. Finally, this approach generalizes to three-dimensional problems in a straight forward manner due to its generic nature.

## Acknowledgments

This work was sponsored in part by NSERC (Government of Canada), the Canada Research Chair Program (Government of Canada).

## References

- [1] Roache PJ. Verification and validation in computational science and engineering. Albuquerque, New Mexico: Hermosa Publishers; 1998.
- [2] Bathe KJ, Ledezma GA. Benchmark problems for incompressible fluid flows with structural interactions. *Comput Struct* 2007;85:628–44.
- [3] Bathe KJ, Zhang H. A mesh adaptivity procedure for cfd and fluid-structure interactions. *Comput Struct* 2009;87:604–17.
- [4] Roache PJ, Ghia K, White F. Editorial policy statement on the control of numerical accuracy. *ASME J Fluids Eng* 1986;108:2.
- [5] Kojic M, Bathe KJ. Studies of finite element procedures? Stress solution of a closed elastic strain path with stretching and shearing using the updated Lagrangian Jaumann formulation. *J Comput Struct* 1987;26:175–9.
- [6] Steinberg S, Roache PJ. Symbolic manipulation and computational fluid dynamics. *J Comput Phys* 1985;57:251–84.
- [7] Bathe KJ. Finite element procedures. Engelwood Cliffs, New Jersey: Prentice-Hall, Inc.; 1996. 07458.
- [8] Pelletier D, Roache PJ. Cfd code verification and the method of manufactured solution. In: 10th Annual conference of the cfd society of Canada, 2002.
- [9] Pelletier D, Roache PJ. In: Minkowycz WJ, Sparrow EM, Murthy JY, editors. Verification and validation of computational heat transfer in handbook of numerical heat transfer. Wiley; 2006 [chapter 13].
- [10] Eça L, Hoekstra M, Hay A, Pelletier D. A manufactured solution for a two-dimensional steady wall-bounded incompressible turbulent flow. *Int Comput Fluid Dynam* 2007;21:175–88.
- [11] Eça L, Hoekstra M, Hay A, Pelletier D. Verification of rans solvers with manufactured solutions. *Eng Comput* 2007;23:253–70.
- [12] Eça L, Hoekstra M, Hay A, Pelletier D. On the construction of manufactured solutions for one and two-equation eddy-viscosity models. *Int J Numer Methods Fluids* 2007;21:175–88.
- [13] Eça L, Hoekstra M. Discretization uncertainty estimation based on a least squares version of the grid convergence index. In: 2nd Workshop on CFD uncertainty analysis, Instituto Superior Técnico, Lisbon, October 2006.
- [14] Salari K, Knupp P. Code verification by the method of manufactured solution. Technical Report SAND2000-1444, Sandia National Laboratories, Albuquerque, NM, 2000.
- [15] Pelletier D. Adaptive finite element computations of complex flows. *Int J Numer Methods Fluids* 1999;31:189–202.
- [16] Pelletier D, Ignat L. On the accuracy of the grid convergence index and the Zhu-Zienkiewicz error estimator. *ASME FED* 1995;213:31–6.
- [17] Etienne S, Pelletier D. An updated Lagrangian monolithic formulation for steady-state fluid-structure interaction problems. In: 43rd AIAA Aerospace sciences meeting and exhibit, Reno, NV, January 2005. AIAA Paper 2004-2239.
- [18] Etienne S, Pelletier D. A general approach to sensitivity analysis of fluid-structure interactions. *J Fluids Struct* 2005;21:169–86.
- [19] Etienne S, Garon A, Pelletier D. Perspective on the geometric conservation law and finite element methods for ale simulations of incompressible flow. *J Comput Phys* 2009;228:2313–33.
- [20] Michler C, van Brummelen EH, de Borst R. An interface Newton–Krylov solver for fluid-structure interaction. *Int J Numer Methods Fluids* 2005;47:1189–95.
- [21] Küttler U, Wall WA. Fixed-point fluid-structure interaction solvers with dynamic relaxation. *Comput Mech* 2008;43:61–72.
- [22] Degroote J, Bathe KJ, Vierendeels J. Performance of a new partitioned procedure versus a monolithic procedure in fluid-structure interaction. *Comput Struct* 2009;87:793–801.